ORIGINAL PAPER

Structural and optical characterization of sol–gel derived boron doped Fe$_2$O$_3$ nanostructured films

C. Aydın · Sh. A. Mansour · Z. A. Alahmed · F. Yakuphanoglu

Abstract Pure and boron (B) doped iron oxide (Fe$_2$O$_3$) nanostructured thin films were prepared by sol–gel spin coating method. The effects of B (0.1, 0.2, 0.5 and 1 %) content on the crystallinity and morphological properties of Fe$_2$O$_3$ films were investigated by X-ray diffractometer and atomic force microscopy. X-ray diffraction patterns revealed that the Fe$_2$O$_3$ films have a rhombohedral crystalline phase of α-Fe$_2$O$_3$ phase (hematite) with nanostructure and their crystallite size (D) is changed from 27 ± 2 to 45 ± 5 nm with B dopant content. The minimum crystallite size value of 27 ± 2 nm was obtained for 0.2 % B doped Fe$_2$O$_3$ film. Carrying out UV–VIS absorption study for both doped and undoped films at room temperature, it was realized that allowed optical transitions may be direct or indirect transitions. The direct and indirect energy gap values for pure Fe$_2$O$_3$ were obtained to be 2.07 and 1.95 eV, respectively. The optical band gap value of the films was changed with 0.1 % B doping to reach 1.86 eV for direct band gap and 1.66 eV in case of indirect band gap.

C. Aydın
Department of Metallurgical and Materials Science, Firat University, Elazig, Turkey

Sh. A. Mansour (✉)
Basic Engineering Science Department, Faculty of Engineering, Menofia University, Shebin El-Kom, Egypt
e-mail: shehab_mansour@yahoo.com

Sh. A. Mansour · F. Yakuphanoglu
Physics Department, Faculty of Science, Firat University, Elazig, Turkey

Z. A. Alahmed
Department of Physics and Astronomy, College of Science, King Saud University, Riyadh 11451, Kingdom of Saudi Arabia

1 Introduction

Iron oxide Fe$_2$O$_3$ (hematite) nanocrystals have attracted a great deal of attention over the past decade. Crystalline Fe$_2$O$_3$ has large applications in chemical industry as active catalytic [1], nonlinear optical materials [2], as photo-electrodes [3] and gas sensors to detect combustible gases like CH$_4$ and C$_3$H$_8$ [4]. Although the physical preparation methods such as chemical vapor deposition (CVD) [5] and laser-assisted CVD [6] result into excellent thin films quality, they have some shortcoming from the point of view of wide usage e.g., lack flexibility and cost effectiveness. Whereas, other methods as sol–gel spin-coating, chemical solution deposition and spray pyrolysis seem to be simpler and economic. Among these methods, sol–gel process is an attractive technique for obtaining film because it has advantages of easy control of the film composition, homogeneity, and large area coating capability. Moreover, this process allows doping of various materials, which makes it possible to fabricate thin, transparent, and multicomponents oxide films.

Nowadays, great attention has to be drawn to the miniaturization of electronic devices. For this reason, surface and interfacial phenomena play an important role in the device performance. One of the main characteristics of the electronic state of the surface is the energy band gap [7]. Iron (III) oxide has a band gap of 2.0–2.1 eV, therefore it can absorb solar radiation from 295 to 600 nm, which comprises 50 % of solar spectrum [8]. Thin films of n-Fe$_2$O$_3$ (with no added metal dopant) have been extensively studied (c.f. [9]) with reported photoconversion

efficiencies of up to 2 % for water-splitting [9–11]. So, adding elements such as B, Al, In and Ga in the substitution of iron atoms can improve the range of solar radiation absorption and the conductivity Fe_2O_3 films. In the present study, we focus on sol–gel synthesis for thin films of pure Fe_2O_3 and doped by boron (B) particularly at 0.1, 0.2, 0.5 and 1 % of B. The variation of energy band gap with different doping concentrations of B in iron oxide thin films were also evaluated.

2 Experimental details

Undoped and B doped nanostructured Fe_2O_3 films were prepared by the sol–gel method onto microscopy glass substrates. Iron chloride hexahydrate ($FeCl_3 \cdot 6H_2O$), boric acid, 2-methoxyethanol ($C_3H_8O_2$) and ethanolamine (C_2H_7NO, EA) were used in preparation. EA was used as a stabilizer and boric acid was used as dopant source. The molar ratio of EA to $FeCl_3 \cdot 6H_2O$ was maintained at 1:1. Firstly, 0.5 M of $FeCl_3 \cdot 6H_2O$ was dissolved 2-methoxyethanol and solution was stirred at 60°C for 1 h. Then, EA was added to this solution to yield a clear and homogeneous solution. The various amounts of boric acid were added to $FeCl_3 \cdot 6H_2O$ to obtain various molar concentrations with 0.1, 0.2, 0.5 and 1 % and then, the solutions were served as the coating source after cooling down to room temperature and ageing for 24 h. For the deposition process of the films onto the microscopy glass substrates, the glass substrates were cleaned in methanol and acetone baths for 10 min using an ultrasonic cleaner, respectively and then, the substrates were rinsed with deionized water and dried with the nitrogen gas. The solutions were coated onto the microscopy glass substrate using spin coater machine at 2,000 rpm for 60 s. After the spin coating, the films were dried at 150 °C for 10 min on a hot plate to evaporate the solvent and to remove organic residuals. The steps from coating to drying were repeated five times to ensure the homogeneity of the deposited films. The obtained thin films were thermally annealed at 400 °C in air for 2 h into a ceramic furnace. The crystal structure of the films were characterized by a Bruker D8 X-ray diffractometer using Cu K_α radiation ($\lambda = 1.5418$ Å) at power of 1,600 W (40 kV, 40 mA). The surface morphology, roughness, and particle size of B-doped Fe_2O_3 thin films were investigated using a Park System XE-100E atomic force microscopy (AFM). The UV–VIS spectra of the films were recorded from 200 to 1,000 nm wavelength using SHIMADZU UV-3600 UV–VIS–NIR spectrophotometer at room temperature.
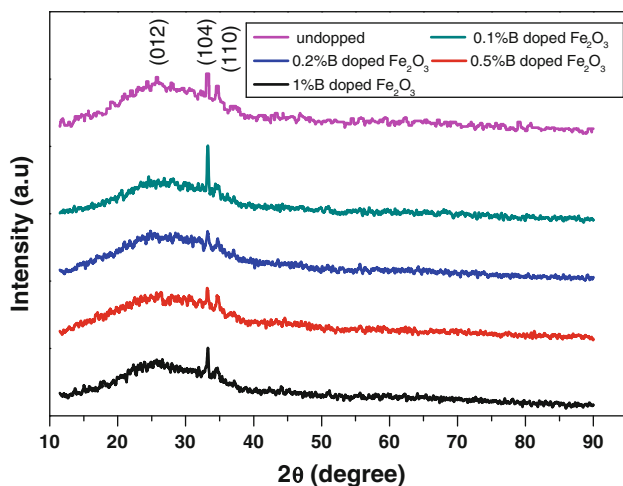
3 Results and discussion

3.1 Structural and morphological characterization of undoped and B-doped Fe_2O_3 nanostructured films

XRD patterns of prepared samples are shown in Fig. 1. All obtained diffraction patterns are assigned well to rhombohedral crystalline phase of α-Fe_2O_3 phase (hematite) in a good agreement with a reference pattern (JCPDS card No. 024-0072 [12]), and its lattice parameters of $a = 0.5038$ nm and $c = 1.3772$ nm. This phase exhibits three maxima intensities at 2θ (Bragg diffraction angle) values 24.12°, 33.107° and 35.611° corresponding to preferential orientations at (012),

**Fig. 1** XRD patterns for undoped and doped Fe_2O_3 nanostructured films

Table 1 Crystal size, average roughness, bandgap (E_g) and both direct and indirect allowed transition energy gap (E_{gd} and E_{gi}, respectively) of undoped and doped Fe_2O_3 nanostructured films

Samples	D (nm)	R_q (nm)	E_g (eV)	E_{gd} (eV)	E_{gi} (eV)
Fe_2O_3	45 ± 5	126.13	2.06	2.07	1.95
0.1 % B doped Fe_2O_3	35 ± 3	131.20	1.88	1.86	1.66
0.2 % B doped Fe_2O_3	27 ± 2	125.34	2.03	2.04	1.92
0.5 % B doped Fe_2O_3	36 ± 3	154.18	2.02	2.01	1.87
1 % B doped Fe_2O_3	39 ± 4	163.95	1.9	1.95	1.72

(104) and (110) planes respectively. The maximum intensity of these three peaks obtained for (104) plane was appeared for all samples, whereas the peak for (012) plane become less pronounced for all boron doped samples compared to that in the undoped one.

It should be worth to notice that, the peak intensity at preferred orientation (104) for 0.1 % B doped sample is greater than that of the undoped one. However, for the other doped samples with boron percentage (>0.1 %) have lower intensities at (104) plane than that of the undoped

Fig. 2 2D and 3D AFM images for a pure Fe_2O_3, b 0.1 %, c 0.2 %, d 0.5 % and e 1 % B-doped Fe_2O_3 films
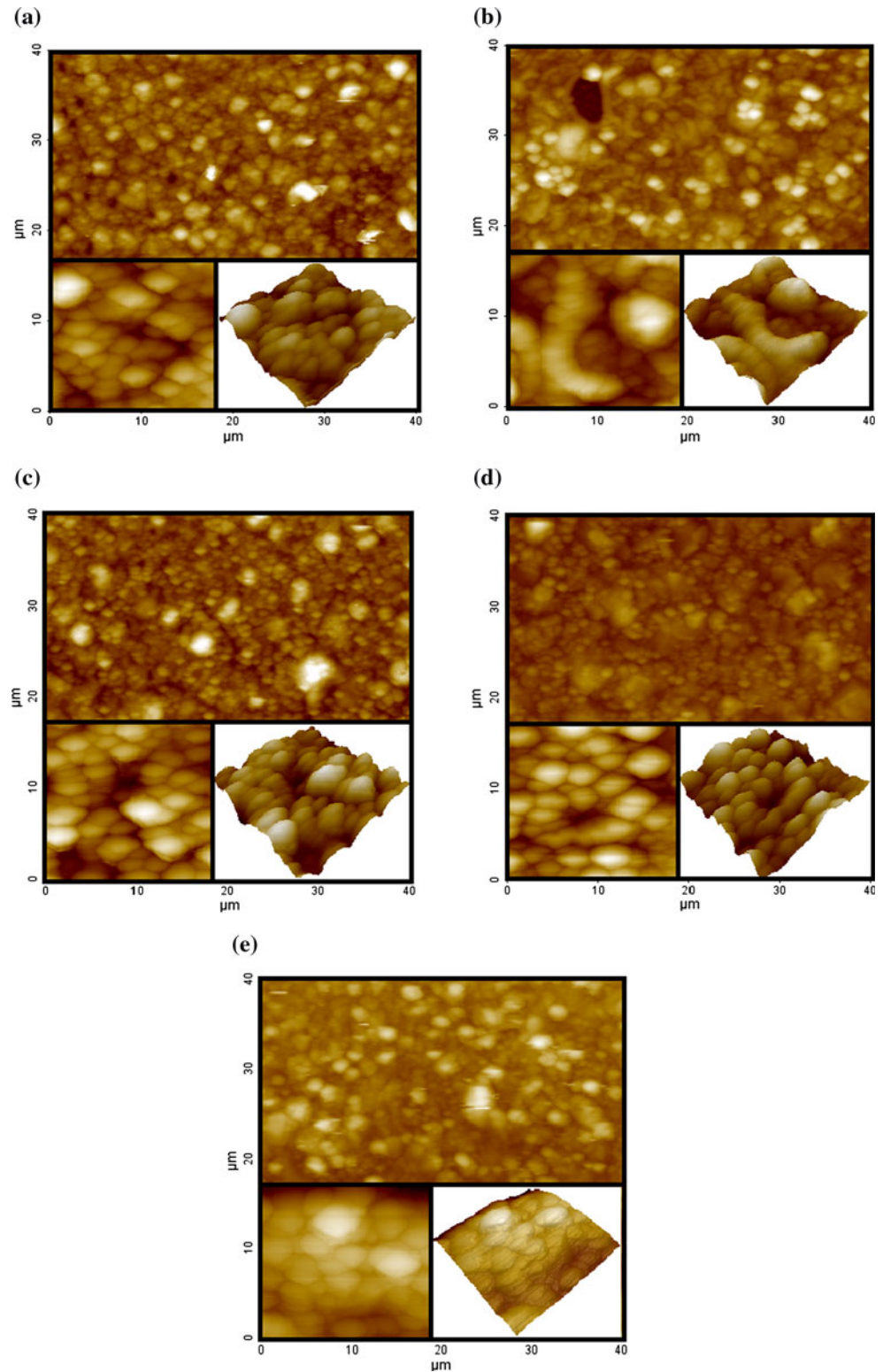
Fe_2O_3 sample. According to XRD results, it is shown that the crystallinity of the Fe_2O_3 films enhanced with 0.1 % boron doping. In contrast, the crystallinity of the Fe_2O_3 films deteriorated with boron incorporation (0.2–1 %). This indicates that higher content of boron leads to a deterioration of the crystal structure by distorting the Fe_2O_3 lattice. Some lattice defects and distortion of the crystal lattice are induced because of differently sized atoms substitute in the Fe_2O_3 lattice [13, 14].

In order to calculate the crystalline size (D), one can use the value of full width at half maximum (FWHM) for the highest intensity diffraction peak (104) using the following known Debye–Scherrer equation [15, 16]:

$$D = \frac{0.9\lambda}{\beta \cos \theta} \qquad (1)$$

where λ, β and θ are the X-ray wavelength, FWHM of the diffraction peak and the Bragg diffraction angle, respectively. The crystal size estimated by Debye–Scherrer formula is given in Table 1. The calculated values of D for the investigated samples varied from 27 ± 2 to 45 ± 5 nm. This indicates that B doped Fe_2O_3 films are nanostructure materials. The obtained values of D are decreased with increase of boron addition up to 0.2 % and increases promptly at 0.5–1 %.

Figure 2 shows the AFM images of Fe_2O_3 films undoped and doped with different doping percentage of B. The AFM images are 2D (40 μm × 40 μm), 2D (5 μm × 5 μm) at left inset and 3D (5 μm × 5 μm) at right inset for all the films. The average roughness R_q, values for the AFM (40 μm × 40 μm) images for each films were determined using a PARK system XEI software programming and are given in Table 1. As seen in Table 1, the R_q values are increased with the boron doping. This indicates that the boron becomes less homogeneously distributed along the film thickness with increasing the boron contents. Also, using a PARK system XEI software programming the values of nano-clusters size and the thicknesses for all the films were determined. The obtained clusters size values were very close to each other and its mean value was found to be 437 ± 1.4 nm. While, the obtained mean value of thickness for all films was found to be about 870 ± 25 nm.

3.2 Optical properties of undoped and B-doped Fe_2O_3 nanostructures

Figure 3 shows the transmittance (T) spectra in the range of 300–850 nm for the undoped and doped Fe_2O_3 films with various doping percentage of B. The average transmittance in the visible region was observed about 65 % for the undoped and doped (from 0.2 to 1 % B) films. Whereas, 0.1 % B doped Fe_2O_3 film shows a lower transmittance than all other films in whole investigated wavelength range. The absorbance (A) spectra of the films are shown in Fig. 4. As seen clearly in Fig. 4, the Fe_2O_3 film doped with 0.1 % B shows the higher absorbance than all other films in whole investigated especially in the strong absorption edge region. The obtained higher value of absorbance ensure that the lowest values of the transmittance for film doped with 0.1 % B not come from scattering due to no smoothing or inhomogeneity of film surface.

The absorption coefficient (α) is plotted versus the photon energy (hv) for pure and doped Fe_2O_3 nanocrystalline films and is shown in Fig. 5. The intercepts of such plot on the photon energy axis give the band gap of each film. It is evident from the Fig. 5 that there is a considerable reduction in the band gap for boron-doped Fe_2O_3 samples with respect to the undoped film. The band gap of
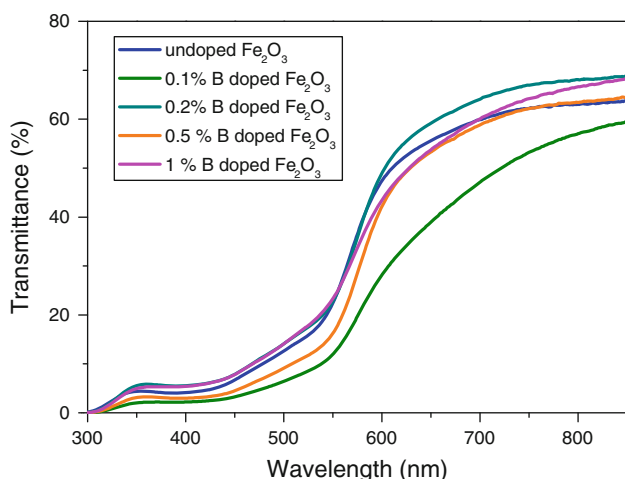

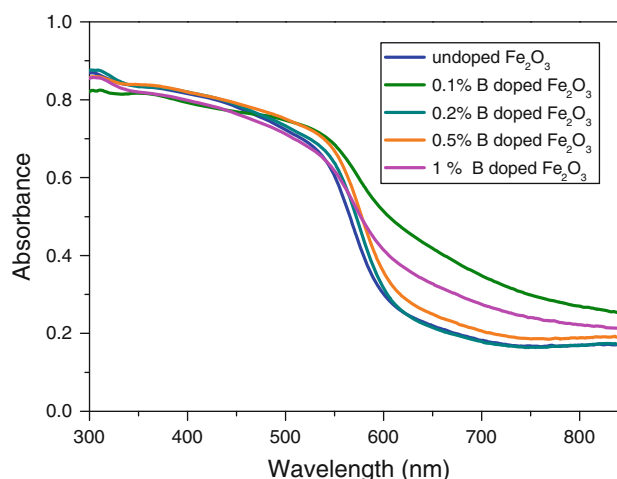**Fig. 3** Transmittance spectra of undoped and B doped Fe_2O_3 films

Fig. 4 Absorbance spectra of undoped and B doped Fe_2O_3 films

pure Fe_2O_3 film is found to be 2.06 eV and which of doped Fe_2O_3 films are in the range from 2.03 to 1.88 eV, as seen in Table 1. The low energy region in Fig. 5 shows an exponential fall for all the presented curves. These exponential edges may be attributed to lack of long-range order or the presence of defects in films [17, 18]. These curves can be characterized by two different slopes indicating the presence of direct and indirect transitions in the materials. In other words, these curves can be characterized by two slopes indicating the presence of both direct and indirect transitions in the undoped and doped films.

For photon energies (hv) just above the fundamental edge, the optical band gap of the films can be determined by the following relation [19]:

$$\alpha hv = \beta (hv - E_g)^m \tag{2}$$

where β^{-1} is the band edge parameter constant and E_g is the optical band gap between the valence band and the conduction band. While m is a number characterizing the transition process which takes values 1/2, 3/2, 2 or more depending on whether the transition is direct or indirect and allowed or forbidden, respectively. In the direct and allowed cases, the index m is 1/2, whereas for the forbidden direct cases, it is 3/2. But for the indirect and

allowed cases $m = 2$ and for the forbidden cases, it is 3 or more [20, 21].

In order to determine the direct and indirect optical band gaps, the plots of $(\alpha hv)^2$ versus hv, and $(\alpha hv)^{1/2}$ versus hv were plotted and are shown in Figs. 6 and 7, respectively. The intercept of the linear portion of these curves on the photon energy axis gives the direct and indirect optical band gaps. The obtained E_g values of the direct and indirect transitions for the pure and doped nanocrystalline Fe_2O_3 films are listed in Table 1. The direct and indirect energy gap values for pure Fe_2O_3 were 2.07 and 1.95 eV, respectively. These values are in good agreement with Fe_2O_3 thin films deposited by spray pyrolysis (2.22 and 1.94 eV for direct and indirect transitions, respectively) determined by Akl [22] and 2.1 eV for direct transition reported by Ouertani et al. [23]. Also, the value of direct energy gap is in quite agreement with the obtained α-Fe_2O_3 films prepared by sol–gel method ($E_g = 2.1$ eV) [24]. Whereas, the obtained value for E_g of direct transition for the pure Fe_2O_3 film (2.07 eV) is less than obtained for mechanically milled Fe_2O_3 nano powder, particle size ~ 40 nm, ($E_g = 2.56$ eV [25]). The variation of the optical band gaps obtained from various plots with boron content are shown in Fig. 8. As seen in Fig. 8, the values of optical
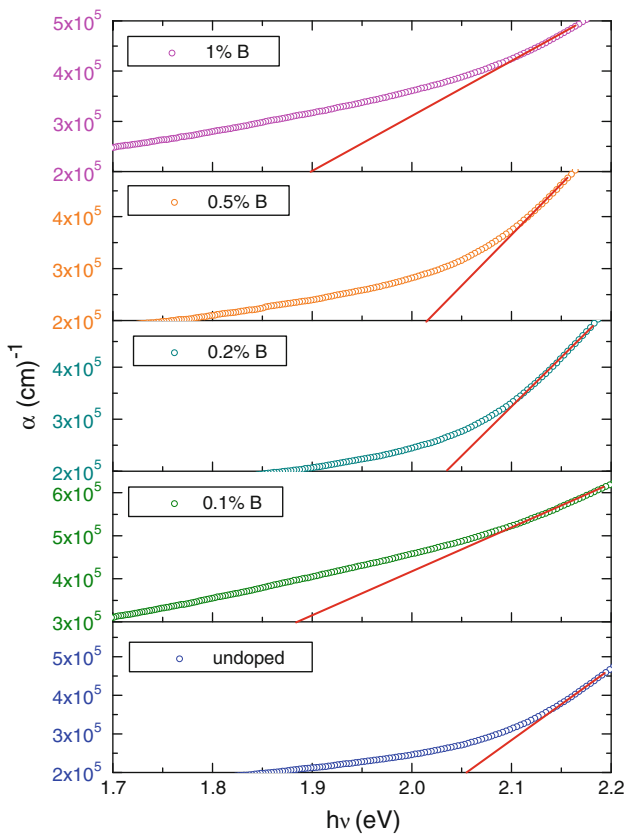

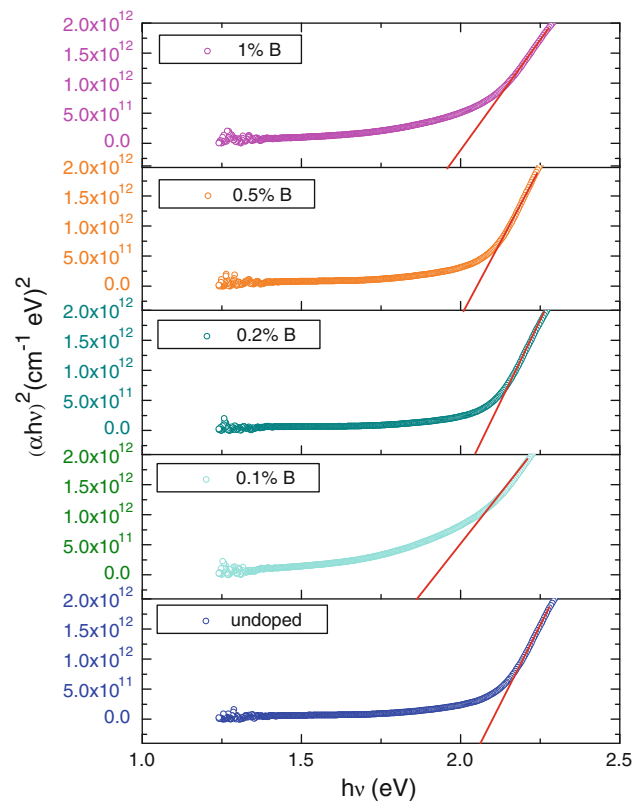**Fig. 5** Plots of α versus hv of undoped and B doped Fe_2O_3 films

Fig. 6 Plots of $(\alpha hv)^2$ versus hv of undoped and B doped Fe_2O_3 films

Fig. 7 Plots of $(\alpha h\nu)^{0.5}$ versus $h\nu$ of undoped and B doped Fe_2O_3 films
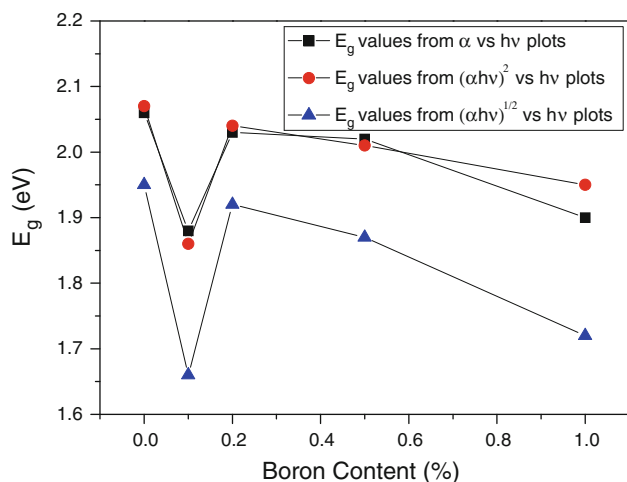
band gap values obtained by different methods as a function of boron doping percentage show the same pattern, i.e., the 0.1 % B doped sample has the lowest value of energy gap for all used methods. In fact, the variation of the optical band gap values for crystalline films can be attributed to [26–28]: (1) a stress induced distortion of the band by the film/substrate interaction, (2) line and planar defects in the crystalline film and (3) the crystalline size which is the effect on band bending at the particle boundaries. Here, the effect of stress induced distortion of the band by the film/substrate interaction in the variation of energy gap could be excluded due to the same film processing conditions for all the films. Thus, the doping by boron into Fe_2O_3 films indicated a considerable effect on crystalline size and followed by defects in crystalline structure.

4 Conclusions

The nanocrystalline undoped and B doped Fe_2O_3 films were prepared using the sol–gel method. XRD results indicate that pure and B-doped Fe_2O_3 samples have rhombohedral crystalline phase of α-Fe_2O_3 phase (hematite) with nanostructured form. The calculated values of crystal size for the investigated films using Debye–Scherrer formula showed that the maximum value of D is 45 ± 5 nm for pure Fe_2O_3 film and other doped samples have the lower values of D without unique trend with B%. The optical band gap values of the films exhibit a considerable reduction with boron doping with respect to the undoped film. The observed variations in the crystal size and optical band gap of the films confirm that the optical and structural parameters of the Fe_2O_3 films derived via sol–gel method can be controlled by boron doping.

Fig. 8 Variation of the obtained E_g values with boron contents

band gap obtained from α versus $h\nu$ plots are very close to the direct energy gap obtained from $(\alpha h\nu)^2$ versus $h\nu$ plots for all the films. As seen in Fig. 8, there is a considerable decrease in the optical band gap for boron-doped Fe_2O_3 samples with respect to the undoped film for all used methods. Moreover, the three presented curves for optical

References

1. Mimura N, Takahara I, Saito M, Hattori T, Ohkuma K, Ando M (1998) Catal Today 45:61
2. Lottici P, Baratto C, Bersani D, Antonioli G, Montenero A, Guarneri M (1998) Opt Mater 9:368
3. Miller EL, Rocheleau RE, Khan S (2004) Int J Hydrogen Energ 29:907
4. Huo L, Li W, Lu L, Cui H, Xi S, Wang J, Zhao B, Shen Y, Lu Z (2000) Chem Mater 12:790
5. Mathur S, Sivakov V, Shen H, Barth S, Cavelius C, Nilsson A, Kuhn P (2006) Thin Solid Films 502:88

6. Sivako V, Petersen C, Daniel C, Shen H, Mücklich F, Mathur S (2005) Appl Surf Sci 247:513

7. Singh H, Rai AK, Satsangi VR (2005) Instrum Sci Technol 33: 21–31

8. Ingler WB Jr, Khan SUM (2004) Thin Solid Films 461:301–308

9. Khan SUM, Akikusa J (2002) Int J Hydrogen Energ 27:863

10. Khan SUM, Akikusa J (1999) J Phys Chem B 103:7184

11. Armelao L, Granozzi G, Tondello E, Colombo P, Principi G, Lottici PP, Antonioli G (1995) J Non Cryst Solids 192–193:435

12. International Centre for Diffraction Data (2002) JCDPS, USA, PCPDFWIN, version 2.3. www.icdd.com

13. Caglar M, Ilican S, Caglar Y, Yakuphanoglu F (2011) J Alloys Compd 509:3177

14. Kim G, Bang J, Kim Y, Rout SK, Ihlwoo S (2009) Appl Phys A 97:821–828

15. Scherrer P (1918) Nachr Ges Wiss Göttingen 26:98–100

16. Langford JI, Wilson AJC (1978) J Appl Cryst 11:102–113

17. Chowdhury FUZ, Bhuiyan AH (2000) Thin Solid Films 360: 69–74

18. Mathai CJ, Saravanan S, Anantharaman MR, Venkitachalam S, Jayalekshmi S (2002) J Phys D Appl Phys 35:2206–2210

19. Urbach F (1953) Phys Rev 92:1434

20. Adachi S (1999) Optical properties of crystalline and amorphous semiconductors. Kluwer, Boston

21. Shumaila, Lakshmi GBVS, Alam M, Siddiqui AM, Zulfequar M, Husain M (2011) Curr Appl Phys 11:217–222

22. Akl AA (2004) Appl Surf Sci 233:307–319

23. Ouertani B, Ouerfelli J, Saadoun M, Ezzaouia H, Bessaïs B (2008) Thin Solid Films 516:8584–8586

24. Hashimoto T, Yamada T, Yoko T (1996) J Appl Phys 80:3184

25. Chakrabarti M, Banerjee A, Sanyal D, Sutradhar M, Chakrabarti A (2008) J Mater Sci 43:4175–4181

26. Leng WJ, Yang CR, Ji H, Zhang JH, Chen HW, Tang JL (2006) J Appl Phys 100:083505

27. Tohge N, Fukuda Y, Minami T (1992) Jpn J Appl Phys Part 1 31:4016

28. Srikant V, Clarke DR (1997) J Appl Phys 81:6357